Controlling Polymersome Surface Topology at the Nanoscale by Membrane Confined Polymer/Polymer Phase Separation

Caterina LoPresti,[†,‡,#] Marzia Massignani,[†,‡] Christine Fernyhough,[§] Adam Blanazs,[†,§] Anthony J. Ryan,[§] Jeppe Madsen,[†,§] Nicholas J. Warren,[†,§] Steven P. Armes,[§] Andrew L. Lewis,[¶] Somyot Chirasatitsin,[⊥] Adam J Engler,[⊥] and Giuseppe Battaglia[†,*]

[†]Department of Biomedical Science, University of Sheffield, Sheffield, U.K., [‡]Biomaterials and Tissue Engineering Group, Department of Engineering Materials, The Kroto Research Institute, University of Sheffield, Sheffield, U.K., [§]Department of Chemistry, University of Sheffield, Sheffield, U.K., [¶]Biocompatibles U.K. Ltd., Farnham, U.K., [⊥]Department of Bioengineering, University of California-San Diego, La Jolla, California, United States. [#]Present address: Merk Serono SpA, 00012 Guidonia Montecelio, Rome, Italy.

ABSTRACT Nature has the exquisite ability to design specific surface patterns and topologies on both the macro- and nanolength scales that relate to precise functions. Following a biomimetic approach, we have engineered fully synthetic nanoparticles that are able to self-organize their surface into controlled domains. We focused on polymeric vesicles or "polymersomes"; enclosed membranes formed *via* self-assembly of amphiphilic block copolymers in water. Exploiting the intrinsic thermodynamic tendency of dissimilar polymers to undergo phase separation, we mixed different vesicle-forming block copolymers in various proportions in order to obtain a wide range of polymersomes with differing surface domains. Using a combination of confocal laser scanning microscopy studies of micrometer-sized polymersomes, and electron microscopy, atomic force microscopy, and fluorescence spectroscopy on nanometer-sized polymersomes, we find that the domains exhibit similar shapes on both the micro- and nanolength scales, with dimensions that are linearly proportional to the vesicle diameter. Finally, we demonstrate that such control over the surface "patchiness" of these polymersomes determines their cell internalization kinetics for live cells.

KEYWORDS: polymersomes · patchy nanoparticles · phase separation · endocytosis

Nature has the ability to design specific surface patterns and topologies over a wide range of length scales that relate to precise function.[1] For example, phospholipids self-assemble to form membranes that control the compartmentalization of many biological components. These membranes have been recently found to display nanometer[2] and micrometer surface domains[3,4] called "rafts", which are thought to be responsible for fundamental cell processes such as budding, fusion, internalization, and receptor transport.[3,5,6] Similarly viral capsids and envelopes are composed of different proteins and phospholipids organized into clusters to accomplish a number of functions that are possible for merely random arrangements,[7−9] such as cell internalization.[10,11] Giant unilamellar vesicles (GUVs), *i.e.*, micrometer-sized vesicles composed of different phospholipids, have been investigated in the past in order to shed light on the dynamics of raft formation in lipid membranes and their effect on budding and fusion phenomena.[12−17] In these examples, phase separation of domains with distinct compositions is usually induced by a mismatch within the phospholipid chains. Recently, Discher and co-workers[18] used polyvalent cations as ionic bridges to induce phase separation between anionic and neutral amphiphilic block copolymers in giant polymeric vesicles, also known as "polymersomes". Polymersomes are enclosed membranes formed *via* the self-assembly of amphiphilic block copolymers in water.[19] They show enhanced mechanical properties and stability compared to liposomes and can be designed to be biocompatible both *in vivo* and *in vitro*, offering efficient encapsulation of either hydrophilic or hydrophobic compounds.[20−24] Polymersomes can be also decorated with proteins or antibodies, either by attaching the active moieties to the hydrophilic brushes[25,26] *via* covalent bonds or by inserting them across the membrane through biomimetic channels.[27−29] Nanometer-sized polymersomes are more desirable for certain biomedical applications, for example, as intracellular delivery vectors for various payloads.[27] Following a biomimetic approach, we have engineered nanometer-sized polymersomes

* Address correspondence to g.battaglia@sheffield.ac.uk.

Received for review September 19, 2010 and accepted February 2, 2011.

Published online February 23, 2011
10.1021/nn102455z

that spontaneously organize their surface into controlled domains.

Exploiting the thermodynamic-driven tendency of binary mixtures of dissimilar polymers to phase-separate, we mixed different vesicle-forming diblock copolymers to obtain polymersomes with surface domains. Different domain patterns were obtained by systematically varying the relative proportions of the two diblock copolymers. Using confocal laser scanning microscopy to study micrometer-sized polymersomes, and atomic force microscopy, fluorescence spectroscopy and transmission electron microscopy to study nanometer-sized polymersomes, we observe domain formation on both length scales. The morphology and dimension of these domains evolve with relatively slow kinetics, leading to completely segregated asymmetric particles (aka "Janus" particles) at predetermined compositions. Furthermore, we compare mixing three different pairs of amphiphilic diblock copolymers, differing either in both hydrophilic and hydrophobic blocks (AB/CD) or in only the hydrophilic blocks (AB/CB) or, finally, in the hydrophobic blocks (AB/AC). These experiments indicate significant differences in the kinetics of coarsening and in the final domain patterns. Finally, we decorate these polymersomes with biomolecules that become confined within phase-separated domains. The biological implications of such decorated domains on cell internalization kinetics are discussed.

RESULTS

Polymersome Topology Analysis. To drive phase separation between two distinct diblock copolymers within the same polymersome we exploited the behavior of a binary mixture of two diblock copolymers differing in the chemical structure of both the hydrophilic and hydrophobic blocks, that is, AB/CD, and also in their molecular weight. In particular, poly(ethylene oxide)-*block*-poly(butylene oxide) (PEO_{16}—PBO_{22}) (M_w = 1910 Da) and poly((2-methacryloyloxy)ethyl phosphorylcholine)-*block*-poly(2-(diisopropylamino)ethyl methacrylate) ($PMPC_{25}$—$PDPA_{70}$) (M_w = 21600 Da) were mixed at different molar ratios to produce both micrometer-and nanometer-sized hybrid polymersomes. The former polymersomes were formed by electroformation (see Methods), while nanometer-sized particles were produced by hydration and mixing, according to well-established protocols.[28,29] To visualize giant polymersomes by confocal laser scanning microscopy (CLSM), $PMPC_{25}$—$PDPA_{70}$ was fluorescently labeled with rhodamine 6G (Rh6G) and PEO_{16}—PBO_{22} was labeled with 7-diethylaminocoumarin-3-carbonyl azide (DEAC). The kinetics of formation of hybrid polymersomes was very slow, probably due to the relatively high molecular weight (and hence reduced chain mobility) of the PMPC—PDPA. Thus, polymer films were left overnight and measurements were started after 12 h. Experiments were carried out at 25 °C. Figure 1a shows CLSM measurements of the fluorescence signals recorded from the equatorial plane of a representative giant hybrid polymersome at x = 50 mol %, corresponding to PMPC—PDPA (yellow channel), PEO—PBO (blue channel), these two merged images and a 3D reconstruction, respectively. Phase-segregated polymersomes are clearly formed after 12 h. In particular, the 3D reconstruction allows identification of the phase-separated domains. Further measurements taken at longer times (up to 36 h) confirm that these "patchy" polymersomes remain stable and that no further change occurs in their domains (Supporting Information, Figure S1).

It is well-known that, given an appropriate balance between the hydrophilic and hydrophobic blocks, amphiphilic block copolymers in contact with water tend to self-assemble into vesicles spontaneously, due to the *hydrophobic effect*.[30] In the present case, the addition of a second amphiphilic block copolymer increases the complexity of the system. Our CLSM measurements on giant polymersomes confirm that, when $PMPC_{25}$—$PDPA_{70}$ and PEO_{16}—PBO_{22} are mixed at a 1:1 molar ratio, hybrid polymersomes are formed and the two block copolymers tend to phase-separate within each polymersome. Thus, in this case, the hydrophobic interactions overcome the repulsion between the two different block copolymer chains, otherwise discrete pure $PMPC_{25}$—$PDPA_{70}$ and pure PEO_{16}—PBO_{22} polymersomes would be expected.

In this work we focused our attention mainly on nanometer-sized polymersomes, since these are extremely promising in terms of their possible biomedical applications. Polymersomes are prepared by hydration and mixing of thin polymer films, followed by sonication in order to obtain unilamellar vesicles.[27] The intensity-average size distribution obtained by DLS is centered at around 200 nm (see Supporting Information). To investigate the kinetics of phase separation, polymersomes were analyzed at different time intervals.

The first method used to characterize the nanometer-sized polymersomes was cryogenic transmission electron microscopy (cryo-TEM). Figure 1b shows a cryo-TEM raw image of $PMPC_{25}$—$PDPA_{70}$/PEO_{16}—PBO_{22} polymersomes prepared at a 1:1 molar ratio (50 mol %) after 1 month and the image manipulation required to enhance the contrast between the different domains. The difference in electron density between the two diblock copolymers was sufficient to visualize the presence of phase-separated domains on the polymersome surface when working at defocus values of between 10 and 40 μm. High magnification images were obtained for individual polymersomes, filtered using a fast Fourier transform (FFT) method in order to remove any background artifacts,[31] and then reported as a color gradient to emphasize the contrast between the two phases (Figure 1b). To characterize nanometer-sized polymersomes, conventional TEM was also used which is a faster and more convenient imaging method. Positive staining of polymersomes was achieved using phosphotungstic acid (PTA) as a selective

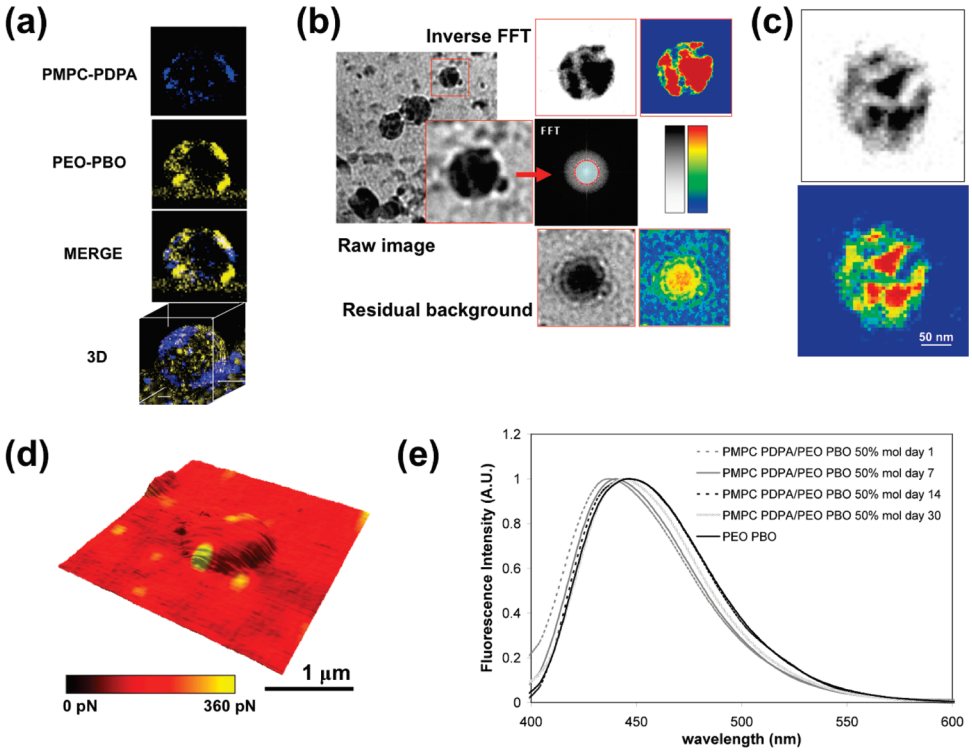

Figure 1. (a) Confocal laser scanning micrographs obtained for a hybrid $PMPC_{25}$—$PDPA_{70}$/PEO_{16}—PBO_{22} polymersome prepared at a 1:1 molar ratio (50 mol %) after 12 h. From top to bottom: equatorial plane from Rh_6G—$PMPC_{25}$—$PDPA_{70}$ channel, equatorial plane from DEAC—PEO_{16}—PBO_{22} channel, merged equatorial plane, 3D image rendering. (b) Cryo-TEM image processing by FFT-filtering of nanometer-sized hybrid polymersomes. (c) FFT-filtered TEM image of a representative hybrid polymersome selectively stained using PTA after 1 month. (d) Force mapping spectroscopy image of adhesive domains (yellow) on a topographical map of a PEO_{16}—PBO_{22}/biotinylated $PMPC_{25}$—$PDPA_{70}$ polymersome prepared at a 1:3 molar ratio (75 mol %), immobilized on a surface and imaged with a streptavidin-functionalized tip after 1 month. (e) Normalized fluorescence spectra recorded for DEAC-labeled hybrid $PMPC_{25}$—$PDPA_{70}$/PEO_{16}—PBO_{22} prepared at a 1:1 molar ratio (50 mol %) polymersomes at different times (dashed lines) and a pure PEO_{16}—PBO_{22} polymersome dispersion.

staining agent for PMPC polymers since this reacts preferentially with ester groups.[32] This functionality is not present in the PEO—PBO copolymers, hence the domains formed by the PMPC—PDPA copolymer appear darker in the TEM images. Figure 1c shows a representative TEM image obtained for a $PMPC_{25}$—$PDPA_{70}$/PEO_{16}—PBO_{22} polymersome prepared at 50 mol % after 1 month after FFT filtering, as described for cryo-TEM images. Phase-separated domains are also confirmed using this technique. Furthermore, the domain morphologies detected by environmental TEM and cryo-TEM are very similar. While EM provides confirmation of phase separation, it does not necessarily confirm the conformation or function of the copolymer within the vesicular structure. To investigate this, polymersomes formed by a mixture of PEO_{16}—PBO_{22} and biotinylated $PMPC_{25}$—$PDPA_{70}$ were immobilized onto an avidin-coated substrate and probed by an atomic force microscope (AFM) tip functionalized with streptavidin protein in buffer (Supporting Information, Figure S2).[33] Only when the avidin coated-tip comes into contact with a biotinylated region of the polymersome surface can substantial binding occur and, upon retraction, the bond ruptures to indicate an adhesion event for a given force. In particular, Figure 1d shows an AFM topology image of a hybrid polymersome with 75% (by mol) biotinylated PMPC—PDPA. The strong interaction between streptavidin and biotin thus allows us to visualize several domains formed by PMPC—PDPA copolymer based on their adhesive interaction with the AFM tip. These adhesion events are indicated by yellow spots confined to the polymersome surface in the overlaid adhesive map, which was obtained at 20 nm lateral resolution. Since receptor—ligand binding is stochastic, a single representative image may only show a subset of the total number of biotin-containing regions that have the appropriate spatial orientation to bind avidin. However, the presence of these domains demonstrates that there is functional biotin on the surface of the polymersome and that it is spatially restricted.

Finally, to investigate whether the segregation is simply confined within the hydrophilic corona of hybrid polymersomes or whether it extends to the inner membrane, hybrid polymersomes were prepared by mixing $PMPC_{25}$—$PDPA_{70}$ with DEAC-labeled PEO_{16}—PBO_{22} prepared at 50 mol % and analyzed using fluorescence spectroscopy. More precisely, DEAC is attached to the *hydrophobic* block, *i.e.*, PBO. It is well-known that aminocoumarin derivatives undergo blue shifts in their emission spectra as the solvent polarity is reduced.[34,35] As PDPA is a less polar environment for DEAC compared to

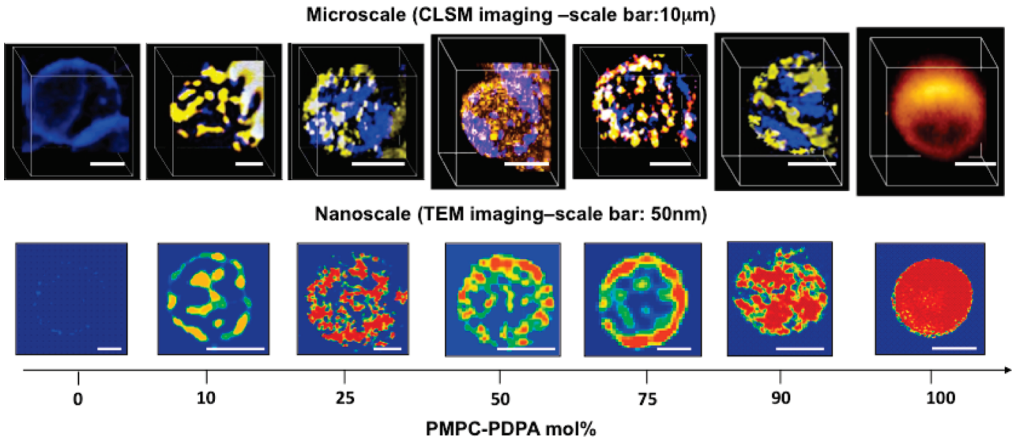

Figure 2. Hybrid $PMPC_{25}-PDPA_{70}/PEO_{16}-PBO_{22}$ polymersomes prepared at different binary compositions. Top: the 3D images calculated from CLSM optical slices showing the microscale morphology. Bottom: the FFT-filtered TEM images obtained for selectively stained polymersomes showing the nanoscale morphology.

PBO, we expect a blue shift in the emission spectra of hybrid polymersomes when the two block copolymers are perfectly mixed in the membrane. Figure 1e shows the normalized emission spectra of hybrid polymersomes excited at 380 nm over time using the pure $DEAC-PEO_{16}-PBO_{22}$ polymersomes as a reference. The emission peak relative to the pure $DEAC-PEO_{16}-PBO_{22}$ polymersomes corresponds to a wavelength of 450 nm and is constant over time. On the other hand, the emission peak of hybrid polymersomes presents a blue shift that reduces over time from $\Delta\lambda = 11$ nm at day 1 to $\Delta\lambda = 1$ nm after 30 days. The reduction of this blue shift is due to an increase in the polarity of the DEAC environment within the membrane over time, which is likely to be related to domain coarsening. PBO blocks, initially mixed with PDPA blocks in the membrane, tend to face other PBO blocks so as to form phase-separated domains. Thus, the environment for DEAC attached to PBO chains tends toward the environment that is characteristic of pure PEO-PBO polymersomes, hence the emission wavelength of hybrid polymersomes becomes closer to the reference. Thus this is reasonable evidence that the phase separation between the $PMPC_{25}-PDPA_{70}$ and $PEO_{16}-PBO_{22}$ chains within hybrid polymersomes also occurs within the hydrophobic membrane and evolves over a time scale of weeks. Further and more detailed considerations regarding the kinetics of domain-coarsening are given in the course of the discussion.

Domain Morphology and Coarsening Kinetics. To investigate the effect of composition on the morphology of segregated domains, both micrometer-sized and nanometer-sized hybrid polymersomes were prepared by mixing $PMPC_{25}-PDPA_{70}$ and $PEO_{16}-PBO_{22}$ at different molar ratios. Figure 2 shows a comparison between CLSM images for micrometer-sized polymersomes recorded after 12 h and TEM images of nanometer-sized polymersomes recorded after 2 weeks at different $PMPC_{25}-PDPA_{70}$ mol %, y. The surface of such hybrid polymersomes is typically spatially segregated at all the investigated compositions, with the "patches" being composed of the minor copolymer component in each case. Different morphologies are obtained by varying the relative copolymer composition and appear similar both at the micro- and nanoscale, suggesting that this phase separation phenomenon has universal character. For $y = 10\%$ and $y = 25\%$ irregular spots are visible, while at $y = 50\%$ and $y = 90\%$ a tendency to form stripes is observed. For $y = 75\%$ the presence of regular circular spots is observed. These features are the result of a subtle balance between several contributions to the overall free energy, such as repulsive interactions, loss of conformational entropy, interfacial energy, and chain stretching over a curved surface. In particular, CLSM allows the detection of shape instabilities and surface inhomogeneities. For example, at $y = 75\%$ the presence of circular PEO−PBO domains as well as bumpy circular PMPC−PDPA domains is visible (Figure 2). At this composition, the PMPC−PDPA chains act as the continuous phase, but the difference in molecular weight between the two hydrophilic blocks is likely to cause shape instabilities due to the differing membrane curvatures.[36] In particular, the higher molecular weight and asymmetry of the PMPC−PDPA may lead to a higher local curvature. Computer simulations carried out by Fraaije *et al.*[37] on polymersomes formed by generic block copolymers comprising the same hydrophilic blocks but differing block lengths show that, when the more asymmetric copolymer is the main component, the formation of shape instabilities, protrusions, and invaginations of the polymersomes can occur so as to minimize contact between domains. Similar phenomena may explain the presence of shape "noise" of the membrane, which is particularly emphasized when PMPC−PDPA is the continuous phase.

Similarly, grain boundary "scars" have been predicted by both mathematical models and also by computer simulations of the self-assembly of various materials,[38−40] due to differing local curvatures at the domain boundaries, regardless of the particular system. Interestingly, morphologies similar to those observed for $y = 25$, 50, and 75%

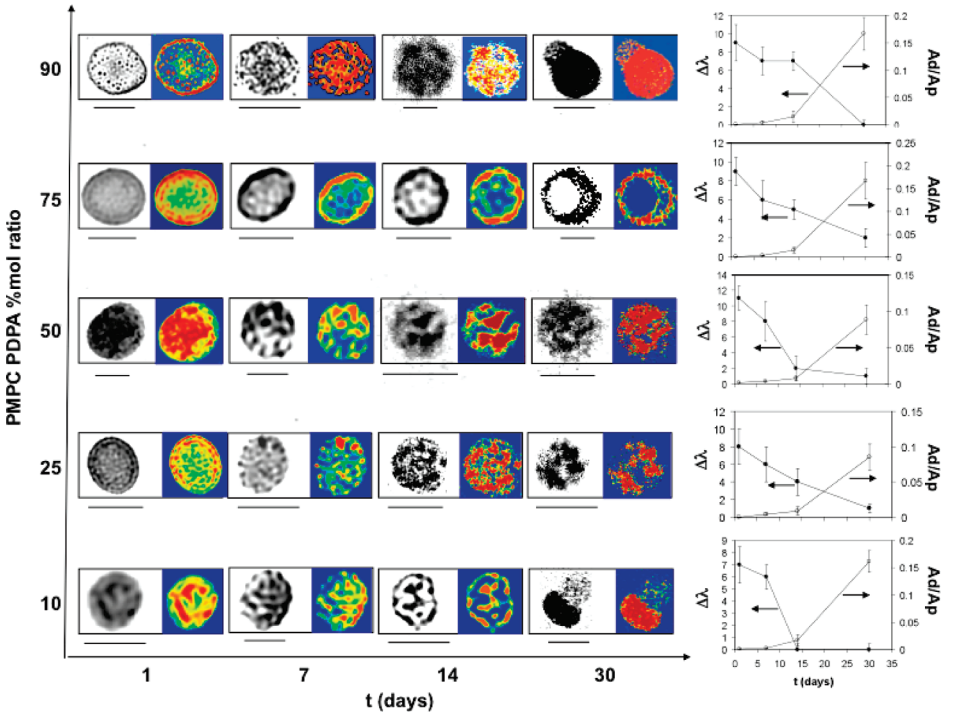

Figure 3. Evolution of the domain coarsening for $PMPC_{25}-PDPA_{70}/PEO_{16}-PBO_{22}$ hybrid polymersomes prepared at different compositions and the corresponding DEAC's emission wavelength shift and single domain to polymersome surface ratio, A_d/A_p, over time. FFT filtered micrographs acquired by TEM using PTA as a selective stain (error bars = SD).

were predicted by simulation of the self-assembly of a single block copolymer on a spherical surface.[38]

TEM images obtained using negative staining (see Methods) confirm phase separation along the membrane, as shown in Figure S3 for a hybrid polymersome prepared at $y = 75$ mol %. Dark regions corresponding to a thickness of approximately 6.0 ± 0.2 nm alternate with bright regions of around 2.5 ± 0.3 nm. These thicknesses are very close to the membrane thicknesses already reported for pure $PMPC_{25}PDPA_{70}$ and $PEO_{16}PBO_{22}$ polymersomes, respectively.[41,42] Similar behavior has been theoretically described by Pata and Dan,[43] who derived a model for the reduction in polymer membrane thickness in the proximity of a relatively short protein inclusion.

To explore the coarsening kinetics of phase-separated domains, we followed the behavior of hybrid polymersomes over time. For micrometer-sized polymersomes, our observations were limited to a time window of 12−24 h after commencing electroformation. In this interval, no appreciable modifications of the domains were observed. While fast coarsening kinetics (seconds to minutes) are generally found for lipid GUVs, relatively slow kinetics were observed for micrometer-sized polymersomes[18] (up to 2 or more days). Here we focused our attention on the coarsening kinetics of domains at the nanoscale. Nanometer-sized hybrid polymersomes were prepared and studied at room temperature over a time-scale of more than 1 month.

Figure 3 shows the TEM images relating to the evolution of PTA-stained $PMPC_{25}-PDPA_{70}/PEO_{16}-PBO_{22}$ hybrid polymersomes prepared at different copolymer compositions over a month, as well as the corresponding variation in the ratio between the single domain area and the polymersome area, A_d/A_p, and the wavelength shift, $\Delta\lambda$, of the maximum fluorescence intensity due to the DEAC label attached to the PBO blocks. At all the analyzed compositions, a clear coarsening of the phase-separated domains became apparent over the observation period, which led to a significant reduction in the total number of domains per vesicle. This corresponds to an increase in the A_d/A_p ratio (and, accordingly, a reduction in the $\Delta\lambda$) since the contact area between PBO and PDPA in the hydrophobic membrane gradually reduces as the two types of diblock copolymer undergo phase separation. After 1 month, the polymersomes prepared using $y = 10$, 25, and 90 mol % evolve to almost completely phase-segregated Janus particles. In particular, for the most asymmetric compositions, that is, $y = 10$ mol % and $y = 90$ mol %, a change in the particle morphology accompanies complete segregation. At the former composition, one budded domain is visible, while at the latter composition the polymersome assumes a "mushroom-like" shape with a cap formed by the minor component. No further modifications in the morphology of either particles or domains are visible after a further month of observation. As already mentioned, a complex balance between different energetic contributions is thought to be responsible for the phase separation phenomena observed for these hybrid polymersomes. In addition, the fact that surface energy prevails over bulk energy at the nanoscale may explain the absence of Janus particles at $y = 50$ mol % and $y = 75$ mol %. For example, it has been observed for various functional materials that, in some cases, frustrated phases

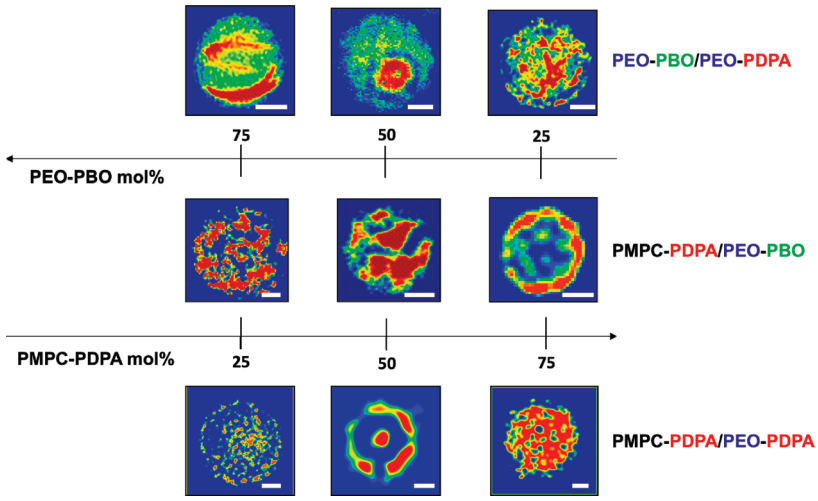

Figure 4. Comparison between TEM images for PEO_{16}—PBO_{22}/$PEO_{23}PDPA_{10}$, $PMPC_{25}$—$PDPA_{70}$/PEO_{16}—PBO_{22} and $PMPC_{25}$—$PDPA_{70}$/PEO_{23}—$PDPA_{10}$ hybrid polymersomes obtained after 14 days. (scale bar = 50 nm).

are visible where the phase transition is arrested below a critical dimension.[44] Modification of the geometry of phase-separated lipid vesicles has been observed[14] in the past as the result of a balance between bending resistance, lateral tension, line tension, and normal pressure as well as elastic compression/stretching and tilt, and hydrophobic height mismatch between the different phases. Here we observe some variation in the polymersome morphology at the most asymmetric compositions (y = 10 mol % and y = 90 mol %) (Figure 3). At y = 90 mol % high local curvature is visible together with the budded PEO-PBO-rich phase, similar to the observations previously reported for phase-separated lipid GUVs.[14] At y = 10 mol % the "mushroom-like" shape of polymersomes may be due to the higher bending rigidity of $PMPC_{25}$—$PDPA_{70}$ chains compared to PEO_{16}—PBO_{22} chains, whose molecular weights are M_w = 21600 Da and M_w = 1910 Da, respectively. In the present case the dimensions of the PMPC—PDPA rich domain is of the order of tens of nanometers, thus it is likely that the local membrane curvature would be too high and not compatible with the rigidity of the PDPA membrane to give rise to a new budded vesicle. The "mushroom-like" shape may be the result of these effects.

On the basis of this morphological observation we also performed a statistical analysis of the polymersome population analyzing multiple TEM images. First of all, we classified the polymersomes as either "patchy" or "nonpatchy". The graph in Figure S4 shows that at the beginning the percentage of polymersomes identified by TEM that present early stage phase separation depends on their composition. Initially, the two phases are mixed and the wavelength shift of the DEAC fluorescence signal, $\Delta\lambda$, is maximized (Figure 3). Phase separation is detected in all the polymersomes aged for both 1 and 2 weeks. After 1 month, the percentage of phase-separated polymersomes is reduced and the $\Delta\lambda$ is almost completely recovered, indicating that the two phases become completely separated. The "nonpatchy" polymersomes present after 1 month are very likely to be budded vesicles composed of one of the two separated phases. The remaining Janus (y = 10, 25, or 90 mol %) or spotted (y = 50, 75 mol %) polymersomes appear to be stable over at least 2 months of observation, and their dimensions lie between 50 and 200 nm. Taking into account that flat domains evolve and would eventually become a complete spherical bud provided that sufficient area is available,[14] only the domains that are present in larger polymersomes are able to bud to form new, smaller vesicles. In all other cases, reduced domain dimensions do not allow complete budding, giving rise to the frustrated morphologies that are observed after 1 month (Figure 3).

Finally, we studied the effect of mixing different pairs of polymersome-forming copolymers on the extent of phase separation and thus on the domain morphology. In particular, we mixed (i) $PMPC_{25}$—$PDPA_{70}$ with a PEO—PDPA amphiphilic block copolymer (PEO_{23}—$PDPA_{10}$, M_w = 5600 Da) so as to obtain AB/CB hybrid polymersomes where the two copolymer share the same hydrophobic block, and (ii) PEO_{16}—PBO_{22} with $PEO_{23}PDPA_{10}$ as to obtain AB/AC hybrid polymersomes where the two copolymers share the same hydrophilic block.

Figure 4 shows a comparison between the TEM images of the three analyzed systems prepared at different compositions after 14 days. Different phase-separated morphologies are formed at the same composition and same aging time when different copolymers are mixed. In particular, the change in $\Delta\lambda$ over time for the DEAC label (data not reported) shows that the PEO_{16}-PBO_{22}/$PEO_{23}PDPA_{10}$ system prepared at either 50 mol % or 75 mol % PEO_{16}—PBO_{22} is fully phase-separated within 14 days. Although the PEO_{16}—PBO_{22}/$PEO_{23}PDPA_{10}$ hybrid systems present the same hydrophilic blocks (PEO) of similar lengths, phase separation is still clearly evident. Thus the main driving force for phase separation confined within polymersomes seems to be differences between the hydrophobic blocks, either in their chemical structure or relative block length.

On the other hand, the various morphologies exhibited by $PMPC_{25}-PDPA_{70}/PEO_{16}-PBO_{22}$ hybrid polymersomes compared to $PEO_{16}-PBO_{22}/PEO_{23}PDPA_{10}$ may be mainly due to the difference in the relative lengths of the hydrophobic blocks, but some contribution from the differing hydrophilic blocks cannot be excluded at this stage, even if such interchain interactions are expected to be attenuated by water.

When the same chemistry of the hydrophobic blocks is maintained, such as in the case of $PMPC_{25}-PDPA_{70}$/ $PEO_{23}PDPA_{10}$ system, phase separation still occurs. Again, this can be due to both the repulsive interactions between the different hydrophilic blocks and/or the mismatch between the hydrophobic block lengths. Clearly, further characterization studies are needed to understand the main driving force for this complex confined phase separation phenomena. Nevertheless, in this study we demonstrate that simply varying either the chemical structure or relative block composition of binary mixtures of the copolymers leads to the formation of hybrid patchy polymersomes.

Domain Effect on Polymersome Cellular Internalization. Polymersomes are finding many applications as delivery vectors for many therapeutics and contrast agents.[27] We have recently reported that pH-sensitive PMPC−PDPA polymersomes are particularly effective in delivering a wide range of agents within live cells by exploiting endocytosis.[45−49] This natural biological process occurs for most eukaryotic cells and controls the uptake of nutrients. Many different mechanisms lead to the controlled acidification of the internalized material within subcellular compartments (endosomes).[50] We have already demonstrated that when PMPC−PDPA or PEO-PDPA polymersomes are internalized *via* endocytosis they undergo controlled disassembly on reaching the acidic endosomal lumen. This, in turn, leads to local temporal endosomal membrane perturbation that is sufficient to enable the polymersome cargo to escape the endosome and diffuse within the cell cytosol.[45−47] We have also reported that such pH-sensitive polymersomes can be used for the cellular delivery of DNA,[45,46] antibodies,[51] small molecules[47] and a wide range of fluorescent probes, including quantum dots.[49]

The endocytosis efficiency (*i.e.*, number of polymersomes per cell over time) is strongly dependent on the polymersome size and surface chemistry, as well as the polymersome topology.[47] As shown in the Supporting Information, Figure S5, we extended our earlier studies by assessing the rate of polymersome uptake by cells as a function of their domain morphology and size, focusing on biomedically relevant PMPC−PDPA/ PEO−PDPA polymersomes. We studied cell internalization kinetics using primary human dermal fibroblast (HDF) cells by both flow cytometry (using fluorescence-activated cell sorting (FACS) analysis) and also UV/visible spectroscopy of cell lysates after various incubation times with polymersomes. FACS measurements allowed the uptake kinetics to be estimated in terms of cell population, that is, how fast polymersomes enter a given cell colony. Spectroscopic studies of cell lysates after incubation with polymersomes allowed quantification of the percentage of the internalized polymersomes applied per cell at different times. To understand the effect of the domain dimensions on the cellular uptake we plotted the time required for each polymersome to achieve 100% uptake by a given cell population (Figure 5a), the percentage of polymersomes internalized with respect of the total amount of the polymersomes incubated when 100% cellular uptake is attained (Figure 5b) and the ratio of these two parameters, which we define as the endocytosis efficiency, as a function of the PMPC−PDPA content (with 0% representing polymersomes comprising purely PEO−PDPA chains). Although both PMPC and PEO polymers are known to be highly protein-repellent[55−59], both sets of data show that PMPC has a very strong cellular interaction on the nanoscale, leading to efficient and fast internalization. Polymersomes were prepared 2 weeks in advance with respect to the cell

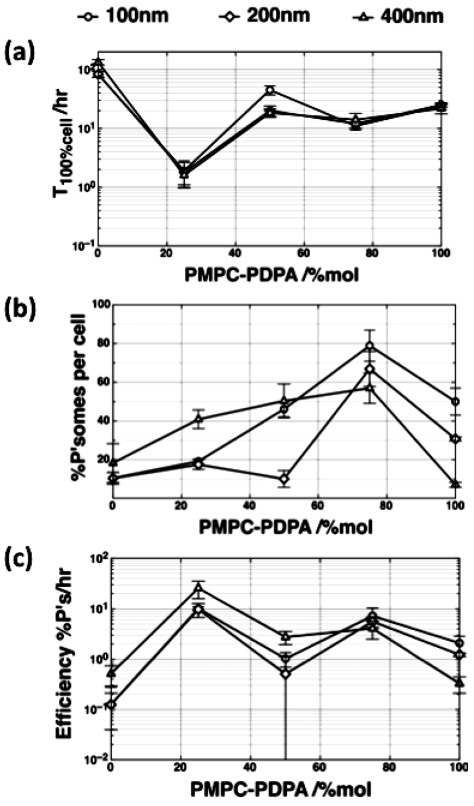

Figure 5. (a) Time required to reach 100% uptake as a function of polymersomes diameter and composition. (b) Percentage of internalized polymersome per cell after 100% cellular uptake is achieved as a function of polymersome diameter and composition. (c) Endocytosis efficiency calculated as the ratio between the percentage of internalized polymersomes to the time required for 100% cellular uptake as a function of polymersome diameter and composition. (Note error bars = SD (n = 3)) Note: the polymersomes were used after 2 weeks from preparation.

incubation experiments. The polymersome size seems to have no effect on how quickly pristine PEO and PMPC polymersomes enter 100% of the cell population (Figure 5a), but it has a remarkable effect on the number of polymersomes internalized per cell (Figure 5b). This latter parameter changes by 3 orders of magnitude on varying the pristine PMPC polymersome diameter from 100 to 400 nm, with the smaller particles being much more efficient. This suggests that PMPC chains have much stronger affinity with the cell surface compared to PEO chains.

When the PEO−PDPA and PMPC−PDPA copolymers are arranged in confined domains, the cellular interaction and the uptake kinetics change dramatically. While the large domain 50/50 (1:1) molar ratio formulation displayed an endocytosis efficiency that was intermediate between the two pristine formulations, both smaller domain 25/75 and 75/25 formulations showed considerably higher endocytosis efficiencies compared to the pure PMPC−PDPA formulations. These two mixed formulations also exhibited different endocytosis profiles: the 25/75 formulation attained 100% cellular uptake within a very short time but the maximum amount of polymersome uptake is relatively low, while the 75/25 formulation reached 100% cellular uptake slightly slower but achieved a higher number of polymersomes per cells. These data suggest that the domain sizes have a strong effect in regulating endocytosis and possibly in controlling the cellular uptake pathway. Further work is ongoing to shed more light on the mechanistic details of polymersome endocytosis. The important point here is that, by controlling the topology of the polymersome surface, we can readily fine-tune their cellular interaction. These results are expected to have a substantial impact on the design of next generation synthetic vectors.

METHODS

$PMPC_{25}$−$PDPA_{70}$ was synthesized and labeled with rhodamine 6G (Rh6G) as described elsewhere.[42] PEO_{16}−PBO_{22} was synthesized as described elsewhere[52] and labeled with 7-diethylaminocoumarin-3-carbonyl azide (DEAC) following the same approach described by Luo *et al.*[53] Synthesis of PEO_{23}−$PDPA_{10}$ has been described previously.[54] Atomic force microscopy-based adhesion force mapping was performed as detailed elsewhere.[33] Briefly, gold-coated, pyramid-shape tips SiN cantilevers with k_{sp} = 20 pN/nm (TR400PB; Olympus; Center Valley, PA) were functionalized (Supporting Information, Figure S1) with streptavidin using a previously established ethanolamine−HCl and bis[sulfosuccinimidyl] substrate method.[55] Biotinylated polymersomes (PEO_{16}−PBO_{22} and biotinylated $PMPC_{25}$−$PDPA_{70}$) were immobilized on avidin-coated coverslips in PBS and placed on an MFP-3D-BIO atomic force microscope (Asylum Research; Santa Barbara, CA). Using custom software written in Igor Pro (Wavemetrics; Portland, OR), samples indented in a regular array of points with 20 nm lateral resolution or 2500 indentations/μm^2 over a scan area of 4 μm^2 and with an indentation velocity of 5 μm/s (~100 nN/s loading rate). To promote biotin−avidin binding, a dwell time of 3 s was added between tip indentation (Supporting Information, Figure S1C; red) and retraction cycles (Figure S1; blue). By knowing the resulting deflection and cantilever spring constant and assuming Hookean behavior for the cantilever, deflection *versus* cantilever position data could be converted into force−indentation spectrographs.[56] Data were then analyzed to determine the maximum adhesive force, that is, the greatest difference between the retraction curve and baseline. Using each force measurement's *x*- and *y*-position, data were then plotted on a map of the surface and interpolated to generate a force spectroscopy map.

Giant polymersomes comprising binary mixtures of $PMPC_{25}$−$PDPA_{70}$ and PEO_{23}−PBO_{10} were prepared by electroformation[28] using a TG315 (TTi) function generator and a homemade electrochemical cell. In particular, $PMPC_{25}$−$PDPA_{70}$ and PEO_{23}−$PDPA_{10}$ were mixed at a predetermined molar ratio using a 2:1 v/v chloroform/methanol solution at 1 mg/mL total copolymer concentration in the organic solvent. The Rh6G-$PMPC_{25}$−$PDPA_{70}$ and DEAC-PEO_{16}−PBO_{22} were added to the above solutions at 5.0 mol % concentration with respect to the total amounts of PMPC−PDPA and PEO-PBO, respectively. Two ITO electrodes of 20 mm length and 3 mm height were coated with 8 μL of the chloroform/methanol copolymer solution and placed in a vacuum oven at 50 °C for 2 h under dynamic vacuum. After drying, the two electrodes were placed in a Petri dish at a distance of 5 mm, and an *ac* voltage of 1.4 V was applied at 10 Hz while 6 mL of PBS buffer solution (pH 7.4) was gradually added. After this addition, the voltage was increased up to 5.5 V at 10 Hz and held constant until the end of the experiment. The surface of the electrodes was analyzed with a LSM 510 Zeiss CLSM instrument, exciting the samples at 488 nm with an argon laser and at 543 nm with a HeNe laser, with synchronous scanning of the sample. 3D images of the giant vesicles were reconstructed by scanning different slices of the samples at different heights.

Nanometer-sized polymersomes were formed by the "swelling and stirring" method.[42] The appropriate block copolymers were dissolved and premixed at different molar ratios in 2:1 v/v chloroform/methanol at 10 mg/mL total copolymer concentration in the organic solvent. DEAC−PEO_{16}−PBO_{22} was added to the above solutions at 5.0 mol % concentration with respect to the total amounts of the PMPC−PDPA and PEO−PBO copolymers, respectively. $PMPC_{25}$−$PDPA_{70}$/PEO_{23}−$PDPA_{10}$ polymersomes were obtained by drying the copolymer solutions in a vacuum oven at 50 °C overnight and adding 0.1 M PBS (pH 7.4) to the films at a copolymer concentration of 5 mg/mL. The aqueous dispersions were stirred with a magnetic stirrer at 2000 rpm for 24 h and finally sonicated for 10 min. For flow cytometry experiments, polymersomes were extruded using a Liposofast extruder.

Cryogenic transmission electron microscopy analyses were carried out using a FEI Tecnai G2 Spirit TEM microscope at 120 kV varying the defocus between 10 and 40 μm. A 3 μL portion of each sample of polymersome/PBS dispersion was deposited onto holey carbon grids at 80% humidity and 25 °C, blotted for 2 s with filter paper, and vitrified in liquid ethane with a Vitrobot (FEI) system.

Polymersomes were stained for TEM imaging using a phosphotungstic acid (PTA) solution prepared dissolving 37.5 mg of PTA in boiling distilled water (5 mL). The pH was adjusted to 7.0 by adding a few drops of 5 M NaOH with continuous stirring. The PTA solution was then filtered through a 0.2 μm filter. Then 5 μL of polymersome/PBS dispersion diluted 10-fold (0.5 mg/mL) was deposited onto glow-discharged copper grids. After 1 min, the grids were blotted with filter paper and then immersed into the PTA staining solution for 20 s for negative staining and 5 s for positive staining. Then the grids were blotted again and dried under vacuum for 1 min. TEM images were taken using a FEI Tecnai G2 Spirit TEM microscope at 80 kV. The average surface of the polymersome domains was measured by image analysis using Gatan Digital Micrograph software.

Fluorescence spectra of 10-fold diluted polymersome dispersions containing a constant amount of DEAC-PEO_{16}-PBO_{22} were acquired with a Cary Eclipse Varian spectrofluorimeter by exciting the samples at 380 nm. All the spectra were zeroed at 650 nm and normalized relative to the maximum emission wavelength.

Primary human dermal fibroblasts (HDF) were isolated from skin obtained from abdominoplasty or breast reduction operations (according to local ethically approved guidelines, NHS Trust, Sheffield, UK). Primary cultures of fibroblasts were established as previously described.[57] Briefly, the epidermal layer of the skin was removed by trypsinization, and the remaining dermal layer was washed in PBS. The dermis was then minced using surgical blades and incubated in 0.5% (w/v) collagenase A at 37 °C overnight in a humidified CO_2 incubator. A cellular pellet was collected from the digest and cultured in (Dulbecco Modified Eagle Media) DMEM (Sigma, UK) supplemented with 10% (v/v) fetal calf serum, 2 mM L-glutamine, 100 IU/ml penicillin, 100 mg/mL streptomycin and 0.625 μg/mL amphotericin B. Cells were subcultured routinely using 0.02% (w/v) EDTA and used for experimentation between passages 4 and 9. Cells were incubated with 2 week-aged polymersomes that varied in both size and copolymer ratio. After different incubation times cells were washed three times in PBS to remove all the unbound polymersomes and subsequently trypsinized (using trypsin-EDTA). The cells were resuspended in PBS and analyzed using a BD FACSArray (532 nm laser min: 10000 cells per measurement).

Supporting Information Available: Additional figures as described in the text. This material is available free of charge *via* the Internet at http://pubs.acs.org.

Acknowledgment. The authors would like to thank the EPSRC (EP/E03103X/1) for funding this work.

REFERENCES AND NOTES

1. Alberts, B.; Johnson, A.; Lewis, J.; Raff, M.; Roberts, K.; Walter, P. *Mol. Biol. Cell*; 4th ed.; Garland Science: New York, 2002.
2. Eggeling, C.; Ringemann, C.; Medda, R.; Schwarzmann, G.; Sandhoff, K.; Polyakova, S.; Belov, V. N.; Hein, B.; von Middendorff, C.; Schönle, A..; *et al*. Direct Observation of the Nanoscale Dynamics of Membrane Lipids in a Living Cell. *Nature* **2009,** *457*, 1159–1162.
3. Simons, K.; Ikonen, E. Functional Rafts in Cell Membranes. *Nature* **1997,** *387*, 569–572.
4. Gaus, K.; Gratton, E.; Kable, E. P. W.; Jones, A. S.; Gelissen, I.; Kritharides, L.; Jessup, W. Visualizing Lipid Structure and Raft Domains in Living Cells with Two-Photon Microscopy. *Proc. Natl. Acad. Sci. U.S.A.* **2003,** *100*, 15554–15559.
5. Jacobson, K.; Mouritsen, O. G.; Anderson, R. G. W Lipid Rafts: At a Crossroad between Cell Biology and Physics. *Nat. Cell Biol.* **2007,** *9*, 7–14.
6. Anderson, R. G. W.; Jacobson, K. A. Role for Lipid Shells in Targeting Proteins to Caveolae, Rafts, and Other Lipid Domains. *Science* **2002,** *296*, 1821–1825.
7. Huiskonena, J. T.; Butchera, S. J Membrane-Containing Viruses with Icosahedrally Symmetric Capsids. *Curr. Opin. Struct. Biol.* **2007,** *17*, 229–236.
8. Grunewald, K.; Desai, P.; Winkler, D. C.; Heymann, J. B.; Belnap, D. M.; Baumeister, W.; Steven, A. C Three-Dimensional Structure of Herpes Simplex Virus from Cryo-Electron Tomography. *Science* **2003,** *302*, 1396–1398.
9. Cockburn, J. J. B.; Abrescia, N. G. A.; Grimes, J. M.; Sutton, G. C.; Diprose, J. M.; Benevides, J. M.; Thomas, G. J.; Bamford, J. K. H.; Bamford, D. H.; Stuart, D. I. Membrane Structure and Interactions with Protein and DNA in Bacteriophage PRD1. *Nature* **2004,** *432*, 122–125.
10. Marsh, M.; Helenius, A Virus Entry: Open Sesame. *Cell* **2006,** *124*, 729–740.
11. Dimitrov, D. S Virus Entry: Molecular Mechanisms and Biomedical Applications. *Nat Rev Microbiol* **2004,** *2*, 109–22.
12. Dietrich, C.; Bagatolli, L. A.; Volovyk, Z. N.; Thompson, N. L.; Levi, M.; Jacobson, K.; Gratton, E. Lipid Rafts Reconstituted in Model Membranes. *Biophys. J.* **2001,** *80*, 1417–1428.
13. Lipowsky, R. Budding of Membranes Induced by Intramembrane Domains. *J. Phys. II France* **1992,** *2*, 1825–1840.
14. Baumgart, T.; Hess, S. T.; Webb, W. W. Imaging Coexisting Fluid Domains in Biomembrane Models Coupling Curvature and Line Tension. *Nature* **2003,** *425*, 821–824.
15. Yanagisawa, M.; Imai, M.; Taniguchi, T. Shape Deformation of Ternary Vesicles Coupled with Phase Separation. *Phys. Rev. Lett.* **2008,** *100*, 148102.
16. Korlach, J.; Schwille, P.; Webb, W. W.; Feigenson, G. W Characterization of Lipid Bilayer Phases by Confocal Microscopy and Fluorescence Correlation Spectroscopy. *Proc. Natl. Acad. Sci. U.S.A.* **1999,** *96*, 8461–8466.
17. Veatch, S. L.; Keller, S. L. Separation of Liquid Phases in Giant Vesicles of Ternary Mixtures of Phospholipids and Cholesterol. *Biophys. J.* **2003,** *85*, 3074–3083.
18. Christian, D. A.; Tian, A.; Ellenbroek, W. G.; Levental, I.; Rajagopal, K.; Janmey, P. A.; Liu, A. J.; Baumgart, T.; Discher, D. E. Spotted Vesicles, Striped Micelles, and Janus Assemblies Induced by Ligand Binding. *Nat. Mater.* **2009,** *8*, 843–849.
19. Discher, B. M.; Won, Y.-Y.; Ege, D. S.; Lee, J. C.-M.; Bates, F. S.; Discher, D. E.; Hammer, D. A. Polymersomes: Tough Vesicles Made from Diblock Copolymers. *Science* **1999,** *284*, 1143–6.
20. Discher, D. E.; Eisenberg, A. Polymer Vesicles . *Science* **2002,** *297*, 967.
21. Lomas, H.; Canton, I.; MacNeil, S.; Du, J.; Armes, S. P.; Ryan, A. J.; Lewis, A. L.; Battaglia, G. Biomimetic pH Sensitive Polymersomes for Efficient DNA Encapsulation and Delivery. *Adv. Mater.* **2007,** *19*, 4238–4243.
22. Lomas, H.; Massignani, M.; Abdullah, A. K.; LoPresti, C.; Canton, I.; MacNeil, S.; Du, J.; Blanazs, A.; Madsen, J.; Armes, S. P..; *et al.* Noncytotoxic Polymer Vesicles for Rapid and Efficient Intracellular Delivery. *Faraday Discuss.* **2008,** *139*, 133–159.
23. Ahmed, F.; Pakunlu, R. I.; Srinivas, G.; Brannan, A.; Bates, F.; Klein, M. L.; Minko, T.; Discher, D. E. Shrinkage of a Rapidly Growing Tumor by Drug-Loaded Polymersomes: pH-Triggered Release through Copolymer Degradation. *Mol. Pharm.* **2006,** *3*, 340–350.
24. Ahmed, F.; Pakunlu, R. I.; Brannan, A.; Bates, F.; Minko, T.; Discher, D. E. Biodegradable Polymersomes Loaded with both Paclitaxel and Doxorubicin Permeate and Shrink Tumors, Inducing Apoptosis in Proportion to Accumulated Drug. *J. Controlled Release* **2006,** *116*, 150–158.
25. Christian, N. A.; Milone, M. C.; Ranka, S. S.; Li, G.; Frail, P. R.; Davis, K. P.; Bates, F. S.; Therien, M. J.; Ghoroghchian, P. P.; June, C. H..; *et al*. Tat-Functionalized Near-Infrared Emissive Polymersomes for Dendritic Cell Labeling. *Bioconjugate Chem.* **2007,** *18*, 31–40.
26. Pang, Z.; Lu, W.; Gao, H.; Hu, K.; Chen, J.; Zhang, C.; Gao, X.; Jiang, X.; Zhu, C Preparation and Brain Delivery Property of Biodegradable Polymersomes Conjugated with OX26. *J. Controlled Release* **2008,** *128*, 120–127.
27. LoPresti, C.; Lomas, H.; Massignani, M.; Smart, T.; Battaglia, G. Polymersomes: Nature Inspired Nanometer Sized Compartments. *J. Mater. Chem.* **2009,** *19*, 3576–3590.
28. Angelova, M. I.; Dimitrov, D. S. Liposome Electroformation. *Faraday Discuss.* **1986,** *81*, 303.
29. Menger, F. M.; Angelova, M. I. Giant Vesicles: Imitating the Cytological Processes of Cell Membranes. *Acc. Chem. Res.* **1998,** 789–797.
30. Israelachvili, J. N. *Intermolecular & Surface Forces*; 9th ed.; Elsevier Science Imprint: London, 2002; p 450.
31. Bracewell, R. N. *The Fourier Transformation and Its Applications*; McGraw-Hill Book Company: New York, 1965; p 640.
32. Gedde, U. W. *Polymer Physics*; Chapman & Hall: London, 1996; p 298.
33. Chirasatitsin, S.; Engler, A. J Detecting Cell-Adhesive Sites in Extracellular Matrix Using Force Spectroscopy Mapping. *J. Phys.: Condens. Matter* **2010,** *22*, 194102.
34. Raju, B. B.; Costa, S. M. B. The Role of Molecular Size in the Excited State Behaviour of Aminocoumarin Dyes in Restricted Media-2: Study of BC I in AOT-Formamide Reversed Micelles. *Spectrochim. Acta A* **2000,** *56*, 1703–1710.
35. Han, W.; Liu, T.; Himo, F.; Toutchkine, A.; Bashford, D.; Hahn, K. M.; Noodleman, L. Theoretical Study of the UV/Visible Absorption and Emission Solvatochromic Properties of Solvent-Sensitive Dyes. *Chem. Phys. Chem.* **2003,** *4*, 1084–1094.
36. Terreau, O.; Luo, L.; Eisenberg, A. Effect of Poly(acrylic acid) Block Length Distribution on Polystyrene-*b*-Poly(acrylic acid) Block Copolymer Aggregates in Solution 2. A Partial Phase Diagram. *Langmuir* **2003,** *19*, 5601–5607.

37. Fraaije, J. G. E. M.; vanSluis, C. A.; Kros, A.; Zvelindovsky, A. V.; Sevink, G. J. A. Design of Chimaeric Polymersomes. *Faraday Discuss.* **2005,** *128*, 355–361.
38. Chantawansri, T. L.; Bosse, A. W.; Hexemer, A.; Ceniceros, H. D.; Gracia-Cervera, C. J.; Kramer, E. J.; Fredrickson, G. H. Self-Consistent Field Theory Simulations of Block Copolymer Assembly on a Sphere. *Phys. Rev. Lett. E* **2007,** *75*, 031802.
39. Bausch, A. R.; Bowick, M. J.; Cacciuto, A.; Dinsmore, A. D.; Hsu, M. F.; Nelson, D. R.; Nikolaides, M. G.; Travesset, A.; Weitz, D. A Grain Boundary Scars and Spherical Crystallography. *Science* **2003,** *299*, 1716–1718.
40. Bowick, M. J.; Cacciuto, A.; Nelson, D. R.; Trevesset, A. *Phys. Rev. Lett. B* **2006,** *73*, 024115.
41. Battaglia, G.; Ryan, A. J. Bilayers and Interdigitation in Block Copolymer Vesicles. *J. Am. Chem. Soc.* **2005,** *127*, 8757–8764.
42. Du, J.; Tang, Y.; Lewis, A. L.; Armes, S. P. pH-Sensitive Vesicles Based on a Biocompatible Zwitterionic Diblock Copolymer. *J. Am. Chem. Soc.* **2005,** *127*, 17982–17983.
43. Pata, V.; Dan, N. The Effect of Chain Length on Protein Solubilization in Polymer-Based Vesicles (Polymersomes). *Biophys. J.* **2003,** *85*, 2111–2118.
44. Saxena, A.; Aeppli, G. Phase Transitions at the Nanoscale in Functional Materials. *MRS Bull.* **2009,** *34*, 804–810.
45. Lomas, H.; Canton, I.; MacNeil, S.; Du, J.; Armes, S. P.; Ryan, A. J.; Lewis, A. L.; Battaglia, G. Biomimetic pH Sensitive Polymersomes for Efficient DNA Encapsulation and Delivery. *Adv. Mater.* **2007,** *19*, 4238–41.
46. Lomas, H.; Massignani, M.; Abdullah, K. A.; Canton, I.; Lo Presti, C.; MacNeil, S.; Du, J. Z.; Blanazs, A.; Madsen, J.; Armes, S. P..; *et al*. Noncytotoxic Polymer Vesicles for Rapid and Efficient Intracellular Delivery. *Faraday Discuss* **2008,** *139*, 143–159.
47. Massignani, M.; LoPresti, C.; Blanazs, A.; Madsen, J.; Armes, S. P.; Lewis, A. L.; Battaglia, G. Controlling Cellular Uptake by Surface Chemistry, Size, and Surface topology at the Nanoscale. *Small* **2009,** *5*, 2424–32.
48. Murdoch, C.; Reeves, K. J.; Hearnden, V.; Colley, H.; Massignani, M.; Canton, I.; Madsen, J.; Blanazs, A.; Armes, S. P.; Lewis, A. L..; *et al*.Internalization and Biodistribution of Polymersomes into Oral Squamous Cell Carcinoma Cells In Vitro and In Vivo. *Nanomedicine* **2010,** *5*, 1025–1036.
49. Massignani, M.; Sun, T.; Blanazs, A.; Hearnden, V.; Canton, I.; Desphande, P.; Armes, S.; MacNeil, S.; Lewis, A.; Battaglia, G. Enhanced Fluorescence Imaging of Live Cells by Effective Cytosolic Delivery of Probes. *PLoS One* **2010,** *5*, e10459.
50. Doherty, G. J.; McMahon, H. T. Mechanisms of Endocytosis. *Annu. Rev. Biochem.* **2009,** *78*, 857–902.
51. Battaglia, G.; Massignani, M.; Lewis, A. L. Intracellular Antibody Delivery. WO2009138473, 2009.
52. Ryan, A. J.; Mai, S.-M.; Fairclough, J. P. A.; Hamley, I. W.; Booth, C. Ordered Melts of Block Copolymers of Ethylene Oxide and 1,2-Butylene Oxide. *Phys. Chem. Chem. Phys.* **2001,** *3*, 2961–2971.
53. Luo, L.; Tam, J.; Maysinger, D.; Eisenberg, A. Cellular Internalization of Poly(ethylene oxide)-*b*-Poly(ε-caprolactone) Diblock Copolymer Micelles. *Bioconjugate Chem.* **2002,** *13*, 1259–1265.
54. Blanazs, A.; Massignani, M.; Battaglia, G.; Armes, S. P.; Ryan, A. J. Tailoring Macromolecular Expression at Polymersome Surfaces. *Adv. Funct. Mater.* **2009,** *19*, 2906–2914.
55. Bonanni, B.; Kamruzzahan, A. S. M.; Bizzarri, A. R.; Rankl, C.; Gruber, H. J.; Hinterdorfer, P.; Cannistraro, S Single Molecule Recognition between Cytochrome C 551 and Gold-Immobilized Azurin by Force Spectroscopy. *Biophys. J.* **2005,** *89*, 2783–2791.
56. Rotsch, C.; Jacobson, K.; Radmacher, M. Dimensional and Mechanical Dynamics of Active and Stable Edges in Motile Fibroblasts Investigated by Using Atomic Force Microscopy. *Proc. Natl. Acad. Sci. U.S.A.* **1999,** *96*, 921–926.
57. Ralston, D. R.; Layton, C.; Dalley, A. J.; Boyce, S. G.; Freedlander, E.; Mac Neil, S. The Requirement for Basement Membrane Antigens in the Production of Human Epidermal/Dermal Composites *in Vitro*. *Br. J. Dermatol.* **1999,** *140*, 605–615.